

Implications changing of the CdS window layer thickness on photovoltaic characteristics of n-CdS/i-AgSe/p-CdTe solar cells

E. E. Assem^a, A. Ashour^{a,b}, E. R. Shaaban^{c,*}, A Qasem^c

^aPhysics Department, Faculty of Science, Islamic University, P. O. Box 170, Al Madinah, Saudi Arabia

^bPhysics Department, Faculty of Science, Minia University, 61519, El Minia, Egypt

^cPhysics Department, Faculty of Science, Al-Azhar University, Assuit, 71542, Egypt

Rietveld refinement techniques have been used to investigate the structural characteristics of CdS window layers at various thicknesses in the current study. The structural parameters were improved as the thickness of the CdS-layer was raised, according to XRD patterns. This, in turn, was owing to the increase in the crystal's size for the studied thin layers. For the Ni/n-CdS/i-AgSe/p-CdTe/Pt heterojunction that was successfully fabricated employing an AgSe buffer layer deposited directly on the p-CdTe absorber layer and then the CdS window layer deposited on these mentioned layers, the photovoltaic properties were determined under the dark and illuminated conditions. In dark conditions, from the forward and reverse (current-voltage) data, the essential behavior related to the fabricated devices has been determined. In addition, the heterojunction resistance, the shunt resistance, the series resistance and the rectification rate were all determined. As well, in the illumination case, the open-circuit voltage, the short-circuit current, the fill factor, the power conversion efficiency, (*PCE*), the photoresponsivity, the quantum efficiency, the dependence of generated photocurrent on the light intensity, the dependence of generated photocurrent on wavelength (λ) for the studied solar cells have been computed and discussed.

(Received August 21, 2022; Accepted November 16, 2022)

Keywords: CdS films, Rietveld refinement, Structural parameters, Photoresponsivity, Photovoltaic characterization

1. Introduction

Renewable and solar energy are developing as a viable appropriate response to the world's energy problem, as the world confronts the impending demise of fossil fuels and the terrible pollution generated by the fuels. Among the different methods for producing the sun's energy, solar cells are an efficient method for converting solar energy into usable electrical energy. In 2009, worldwide PV cell and package output were 12.3 GW [1]. One year later, it had risen to more than 20 GW [2].

Semiconductors have received a lot of attention in recent years. The CdS layer is the most fascinating since it has uses in different photovoltaic applications [3-6]. CdS thin layer is commonly employed as a window layer in solar cell applications because it possesses n-type conductivity and an acceptable optical bandgap of roughly 2.45 eV. Furthermore, the CdS layer has high photosensitivity and so plays a key role in solar cells and other photoelectronic applications [7, 8].

Because the CdS layer possesses good optical and structural characteristics that qualify it for usage as optical filters, it is also utilized as an insulator as well as a permeable layer for optical beams. Because of the harmony of these properties, this layer uses in a wide range of applications among that [9, 10]. In polycrystalline thin-film solar cells, absorption in the CdS layer of heterogeneous conduction has been discovered as a substantial contributor to total light loss [11, 12]. However, the loss of light in the window layer due to absorption is not the only effect.

*Corresponding author: esam_ramadan2008@yahoo.com
<https://doi.org/10.15251/CL.2022.1911.825>

Many methods were done for the deposition of CdS thin films such as the thermal evaporation technique [13], sputtering process [10], chemical bath deposition (CBD) [14], spray pyrolysis method [15], metal organic chemical vapor deposition technique (MOCVD) [16], molecular beam epitaxial method [17], electro deposition process [18], photochemical deposition method [19] and so forth.

Bonnet *et al.* [20] created the first experimental CdTe/CdS cell in 1972 with 6 percent efficiency, and researchers have labored tirelessly since then to improve the efficiency of such cells. In 2016, the First Solar Company recorded the greatest CdTe/CdS solar cell efficiency of 22.1 % [21].

The thermally evaporated AgSe thin film's structural and optical characteristics were investigated in depth [22]. The optical bandgap for virgin thin films in this investigation was 1.94 eV. This thin film's bandgap energy makes it perfect for use as a window layer/buffer layer for solar cell applications. The results in this report emphasized that the mentioned AgSe thin layer had n-type conductivity [22].

In our current work, we seek to study the photovoltaic characteristics of generated solar cell devices as follows: Ni (front electrode)/n-(CdS)/i-AgSe (buffer layer)/p-CdTe/Pt (back electrode). As previously indicated, heterojunction CdS/CdTe solar cells with superior structural features and solar energy efficiency have been the subject of contemporary study. Surface barriers and surface/interface recombination, however, restrict the performance of CdTe-based solar cells. Our framework develops CdS layers (window layers) and AgSe layer (buffer layers) in a heterostructure based on CdTe-layer (base material/absorber layer) to avoid the obstacles that represented the surface defects, thus ensuring excellent performance and improving the photoconversion efficiency for fabricated solar cells. At the AgSe/CdTe interface, the carrier transport of the AgSe layer creates additional electron-hole pairs. The high light trapping of the CdS layer improves the performance of the AgSe active layer (300 nm-thickness), thereby improving the performance of the fabricated solar cells. In a nutshell, this study looks into the limits of several heterostructures made of CdS, AgSe, and CdTe. The density of defects at the CdS/CdTe interface, which is solved by adding the AgSe layer (the buffer layer) between the CdS (the window layer) and CdTe layer (as the absorber layer) is recombination centers that reduce the performance of such solar cells. This work deals with determination of the structural parameters according to X-ray data. The study of the photovoltaic properties of the generated device is carried out under dark and light conditions. The current-voltage pathway of the forward and reverse bias is discussed in the dark condition and the characteristic parameters of the fabricated solar cells are calculated in the illumination conditions. Among the most important parameters that were addressed in the case of illumination, the open-circuit voltage, the short-circuit current, the fill factor, the power conversion efficiency, (*PCE*), photoresponsivity, quantum efficiency, the dependence of generated photocurrent on the light intensity, the dependence of generated photocurrent on wavelength (λ).

2. Experimental techniques

In our current work, high purity CdS thin films were deposited onto glass substrates to study the structural properties for this layer at different thicknesses. The detailed method of preparation was included in our newly published research on these layers [23]. On the other hand, the method of preparing the AgSe thin film used as a buffer layer was detailed in our recently published work [22] and also the preparation method of CdTe thin layer was detailed in our work [22]. The XRD analysis was carried out via (Philips X-ray diffractometry (1710) device) for the radiation of $\text{CuK}\alpha$ with wavelength = 0.15418 nm). With the use of the Rietveld technique and GSAS-II software, the XRD findings were evaluated [24].

The heterojunction device in our work was in the corresponding form: the Ni/n-CdS/i-AgSe/p-CdTe/Pt structure. The front electrode contact was created by depositing a semi-transparent grid of platinum (Pt) fingers (100 nm) directly onto the surface of the CdTe thin layer, while the rear contact electrode made from the nickel layer (Ni) with 100 nm thick was linked to CdS thin film. The integral technique was used to evaluate the thermoelectric characteristics of

the CdS thin layers, and then the electromotive force (e.m.f) generated throughout the thin layers was recorded. At both the cold and hot contacts, the thermal (e.m.f) generated throughout the two copper electrodes of Cu-constantan thermocouples was measured in the temperature range of 300–500 K with a Keithley 2400 Source Meter device.

The I – V measurements for the generated device were carried out using a standard circuit (Keithley 610 and 617 as a voltage source and current meter) to determine the current through the heterojunction at various thicknesses of CdS layer. At room temperature, the dark (current-voltage) characteristics were obtained in a completely dark chamber. Under typical test settings, the Keithley 2400 Source Meter device is utilized the global spectra (AM1.5G) to measure the illumination current-voltage (I - V) properties of the solar cell device. The (I - V) features were tested under a specific illumination light source of power ($P_{in}=0.052$ (mW/cm²) to acquire the solar cell parameters. A Chromel-Alumel thermocouple coupled to a digital thermometer was used to immediately detect the temperature. To assess the spectral responsiveness of the fabricated system, a mono-chromometer flawlessly adapted via a rare-gas ion source in the range of (100-1000 nm) was utilized, and an electrometer and power temperature gauge to measure the radiation power for the wavelengths and a DC power source with a voltage in the range of (0-15 V) and current in the range of (0-2 A).

3. Results and discussion

3.1. Structural pathways

Fig. 1 portrays the XRD curves of CdS powder using Rietveld refinement using X'Pert HighScore program. According to this approach, the CdS powder curves demonstrate that the powder material has a hexagonal structure (wurtzite type, JCPDS 10-0454) [24-27].

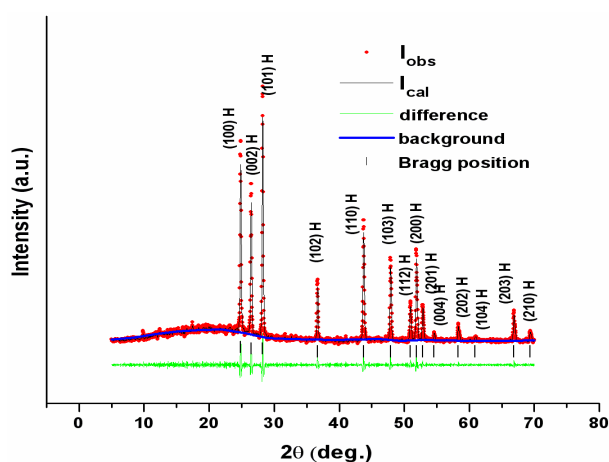


Fig. 1. XRD pattern of CdS powder with Rietveld Refinement.

Fig. 2 displays the XRD of CdS thin layer at different thicknesses. A hexagonal CdS morphology was observed in the handled samples in the thin film form, with crystal planes (100), (002), and (003). (101). As the crystallinity of the film increases, regardless of the processing conditions, increasing the film thickness leads to an increase in peak intensity [28].

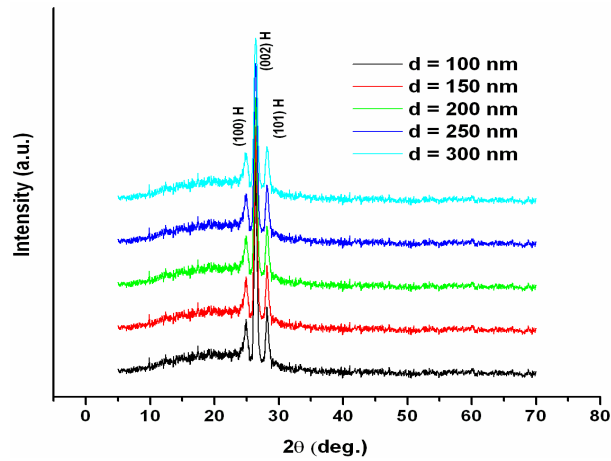


Fig. 2. X-ray diffractograms of the different thickness of CdS thin films.

XRD data are analyzed to estimate the crystallite size, D , and microstrain, ε , of the CdS film with different thicknesses according to the equations of Scherrer $D = 0.9\lambda / \beta \cos \theta$ and Wilson ($\varepsilon = \beta / 4 \tan \theta$) [29-31]. The obtained values of crystallite size, and micro-strain, are listed in Table 1. It is found that with enhance of the thickness the D of the CdS films increments, whereas the micro-strain reduces. The rise in crystallite size indicates a reduction in dislocation density and the defects inside the lattice, resulting in decreasing the inner micro-strain. The thickness-dependent results of CdS thin films are consistent with those found in previous studies [32-34].

Table 1. Values of crystallize size and lattice strain of different thicknesses of CdS thin films.

d (nm)	Cry. Size (nm)	Lattice Str $\times 10^{-3}$
100	16.18	3.95
150	18.98	3.89
200	22.7	3.76
250	25.49	3.56
300	26.58	3.34

3.2. Photovoltaic characteristics

The major parameters of the fabricated solar cells in our report are extracted at different thicknesses of the CdS window layer and using the AgSe as a buffer layer between the window layer and the absorber layer to determine the (I-V) characteristics for the forward and reverse bias under dark and illumination conditions. The diagram of studied n-i-p junction is illustrated in Fig. 3.

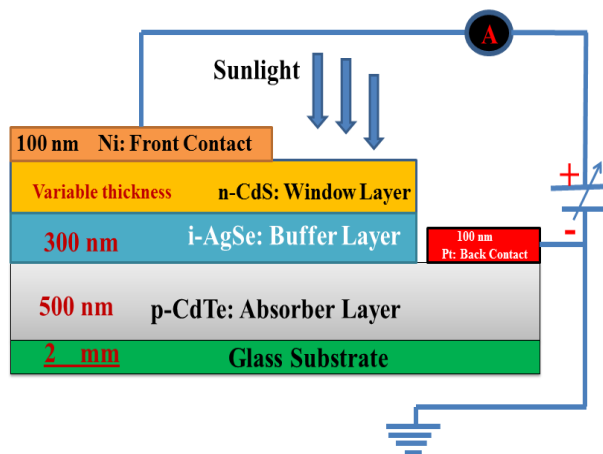


Fig. 3. The diagram of studied n-CdS/i-AgSe/p-CdTe solar cells.

In the generated devices, the current I is linked to the applied voltage V by the following formula [35]:

$$I = I_{01} \left(\exp\left(\frac{q(V - IR_s)}{n_1 k_B T}\right) - 1 \right) + I_{02} \left(\exp\left(\frac{q(V - IR_s)}{n_2 k_B T}\right) - 1 \right) + \left(\frac{V - IR_s}{R_{sh}} \right) \quad (1)$$

In this formula: I_0 symbolizes the saturation current, n epitomizes the quality factor of the fabricated diode), q is the electronic charge which equals to $(1.6 \times 10^{-19} \text{ C})$ and k_B recaps the Boltzmann's constant. The rest parameters in Eq. 1 represent the parasitic resistances which includes the shunt resistance R_{sh} and series resistance R_s .

3.3. Thermoelectric properties of window layers

In a thermoelectric semiconductor, free electrons or holes transport both charge and heat. These charges act in the same way as a gas of charged particles behaves. The amount of an induced thermoelectric voltage in response to a temperature differential across a material, as caused by the Seebeck effect, is measured by the Seebeck coefficient (or thermoelectric power) of that solid. To determine the thermoelectric properties of the window layers in our current study, which leads to knowing the type of conduction prevailing in these layers, we had to measure the Seebeck coefficient, which is by definition the ratio of the potential difference to the temperature difference between the two ends of the studied layers and expresses the Seebeck effect mathematically according to the following equation [36]:

$$S = \frac{\Delta V}{\Delta T} \quad (2)$$

The thermoelectric power (S) has a negative value, suggesting n-type semiconducting activity, as shown in Fig. 4, which depicts the Seebeck coefficient as a function of temperature in the range of 300 to 450 K. The Seebeck coefficient (S) of CdS thin layers as incarnated in the mentioned figure rises with increasing the thin layer thickness and likewise with increasing temperature, as expected for several semiconductors. This finding is consistent with the general rule that increased conductivity results in lower thermoelectric power [37]. On the other hand, the conduction type of CdTe (p-type) and silver selenide (n-type) has been demonstrated in our previous researches [22].

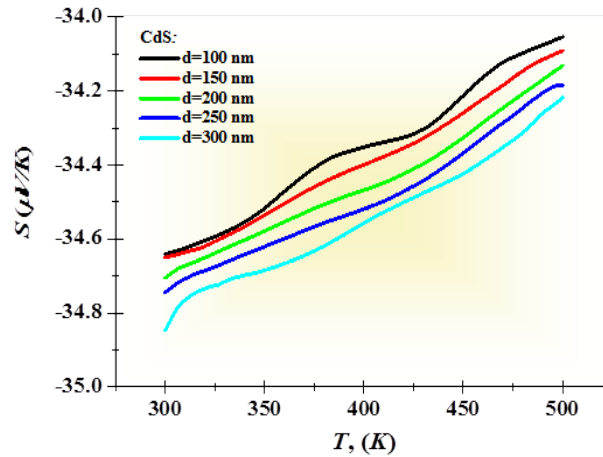


Fig. 4. Seebeck coefficient for the CdS thin layer at different thicknesses.

In a related subject, the concentration of charge carriers n in the window layers, which are electrons, can be calculated using the following relationship [38]:

$$n = \left(\frac{8\pi^2 k_B^2 T m_s^*}{3qh^2} \cdot \left(\frac{\pi}{3}\right)^{2/3} \cdot |S|^{-1} \right)^{1.5} \quad (3)$$

In this equation, k_B portrays the Boltzmann constant ($8.617 \times 10^{-5} \text{ eV / K}$), T is an absolute temperature, $m_s^* = 0.9 m_e = 0.9 \times (9.1 \times 10^{-31} \text{ Kg})$ [38] incarnates the effective mass of the electron, q is the charge of electron ($1.6 \times 10^{-19} \text{ C}$), h represents the Planck's constant ($4.135 \times 10^{-15} \text{ eV / s}$) and $|S|$ is the absolute value of the Seebeck coefficient. The concentration of charge carriers n is plotted in Fig. 5. It is clear that the concentration of charge carriers increases with increasing both the thickness of CdS thin layer and temperature. The electrical characteristics CdS thin layers will enhance as the charge carrier concentration improves [39].

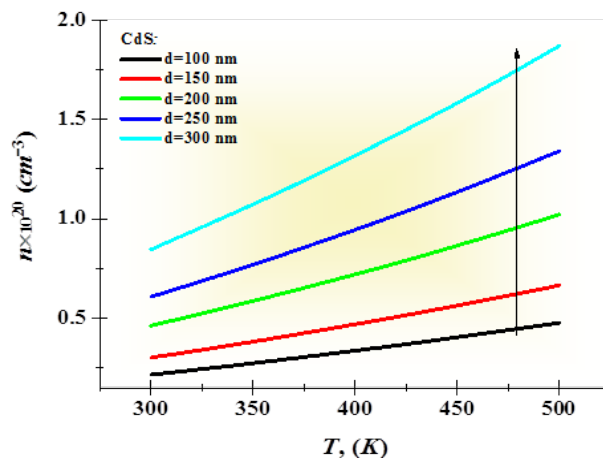


Fig. 5. The concentration of charge carriers for the CdS thin layer at different thicknesses.

3.4. Energy band position of fabricated heterostructure

Firstly, the band structure feasibility of the n-CdS/i-AgSe/p-CdTe heterojunction for solar cell application has been examined. The corresponding positions of the conduction and valence

band edges of CdS (as window layer), AgSe (as buffer layer), and CdTe (as absorber material) are depicted in Fig. 6. The following formulae have been used to obtain the level of energy positions for the valence and conductivity bands (E_{VB} , E_{CB}) for the mentioned layers [40, 41]:

$$\begin{aligned} \Delta E_{CB} &= \left(E_C - X + \frac{E_g}{2} \right) \\ \Delta E_{VB} &= \left(E_C - X - \frac{E_g}{2} \right) \end{aligned} \quad (4)$$

where,

$$X(CdTe) = \left(\left(\frac{E_{EA} + E_{Ion}}{2} \right)_{Cd} \cdot \left(\frac{E_{EA} + E_{Ion}}{2} \right)_{Te} \right)^{0.01} \quad (5)$$

$$X(AgSe) = \left(\left(\frac{E_{EA} + E_{Ion}}{2} \right)_{Ag} \cdot \left(\frac{E_{EA} + E_{Ion}}{2} \right)_{Se} \right)^{0.01} \quad (6)$$

$$X(CdS) = \left(\left(\frac{E_{EA} + E_{Ion}}{2} \right)_{Cd} \cdot \left(\frac{E_{EA} + E_{Ion}}{2} \right)_S \right)^{0.01} \quad (7)$$

In the above equations, E_{EA} portrays the electron affinity of single element or material, E_{Ion} incarnates the first ionization energy, and E_g represents the bandgap energy, (the energy bandgap of CdTe layer and AgSe is 1.45 and 1.94 eV as we mentioned. The (E_{EA} , E_{Ion}) values: for Cd (-0.7, 8.99 eV) [42, 43], Te (1.970, 9.009 eV) [42, 44], S (2.077, 10.36 eV) [45, 46], Ag (1.304, 7.57 eV) [47, 48], Se (2.02, 9.75 eV) [48, 49] and the E_C value is 4.5 eV [50].

Based on the relative positions of the band edges of these layers, fabricated solar cells are all efficient and applicable because the levels of the edges of the energy of all the layers ensure that the energy does not escape and is not lost by the recombination of the different charge carriers in the depletion region. In Fig. 5, the buffer layer (AgSe) has a higher electron affinity compared to the absorber material (CdTe) and this aids to avoid the energy spike at the AgSe/CdTe interface. On the other side, there is also no energy surge at the CdS/AgSe interface (CdS with 100 nm-thickness). This is because the electron affinity for the two mentioned layers is close to each other, as well as the window layer's conductivity is higher than the buffer layer, and the graded junction between them occurs, in which band edges shift over a finite distance with a finite slope proportional to the electric field strength. Furthermore, the n-type CdS at 100 nm-thickness totally exhausts the electrons at the interface, resulting in improved band bending in AgSe, while the p-type CdTe exhausts the holes, resulting in elevated downward bending and the formation of n-CdS/AgSe and AgSe/CdTe interface barriers, as demonstrated in Fig. 6. Moreover, as the voltage drops, the electrons migrate to the p-CdTe region. The holes jump across the barrier at the CdTe/AgSe interface and move into the n-CdS layer. As a result, more charge carriers flow through the heterojunction, increasing the output current for the fabricated device.

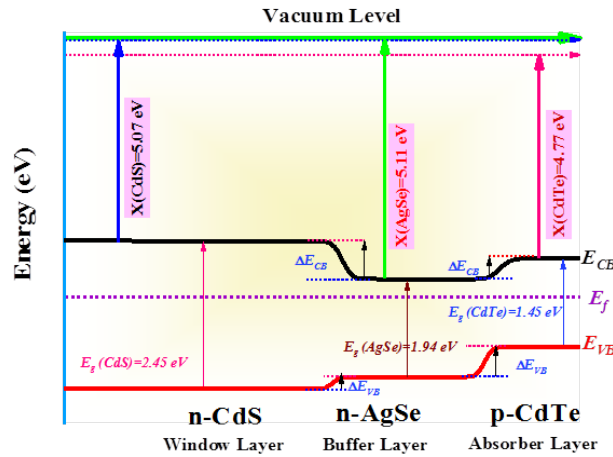


Fig. 6. Energy band diagram of of n-CdS/i-AgSe/p-CdTe heterojunction for CdS-layer with 100 nm.

3.5. The (current-voltage) pathway

Fig. 7 depicts the dark ($I-V$) features for the fabricated device. The current increases as the thickness of the CdS film grows, as shown in this graph. From Fig. 8, it is clear that the current in the forward bias is much greater than the current in the reverse bias, and therefore it can be confirmed definitively on the success of creating solar cells with high efficiency. These graphs show how the forward bias changes the behavior of current for the produced solar cell, which grows considerably in the low voltage area. The exponential behavior in low voltages is due to the growth and production of a depletion area between the CdS thin film produced on the AgSe layer and the CdTe thin film deposited on it. Fig. 9 highlights the fabricated heterojunction resistance according to the $R_j = (\partial V / \partial I)$ relationship [51]. Through this figure, one can discern the values of series resistance R_s and the shunt resistance R_{sh} from the forward and reverse bias as indicated by the arrows in Fig. 9. The values of the mentioned quantities are summarized in Table 2. Observing the behaviour of these parameters, we discovered that they drop as the thickness of the CdS thin layer increases, which is related to the resistance of the heterojunction decreasing as the thickness of this layer increases. On the other hand, Fig. 10 incarnate the rectification ratio, (RR) extracted according to the $RR = (I_F / I_R)_{V=const.}$ formula [52]. It must be noted that in the depletion layer, i.e. in the low voltage zone, the exponential behavior of the reverse current of the studied produced solar cell is smaller than the exponential behavior of the forward current in the same region. As a result, the produced solar cell may be described as having excellent rectification properties [51-53].

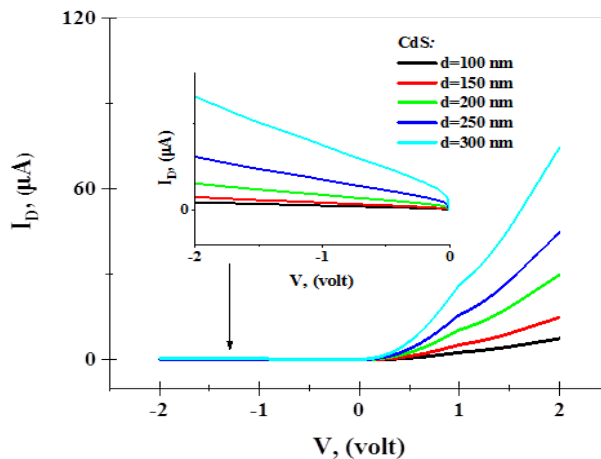


Fig. 7. The dark ($I-V$) characteristics for the fabricated solar cells.

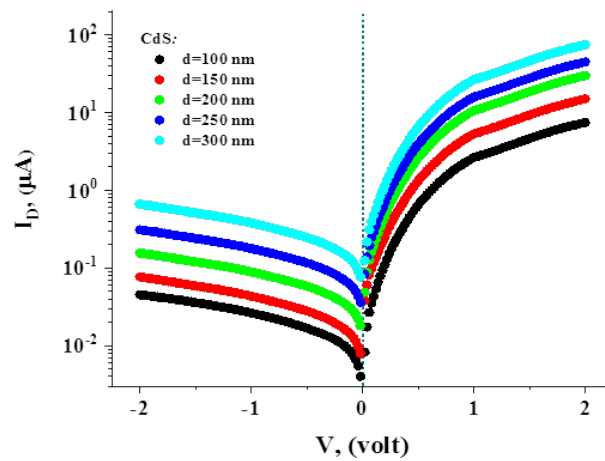


Fig. 8. Current versus the applied voltage for the fabricated solar cells.

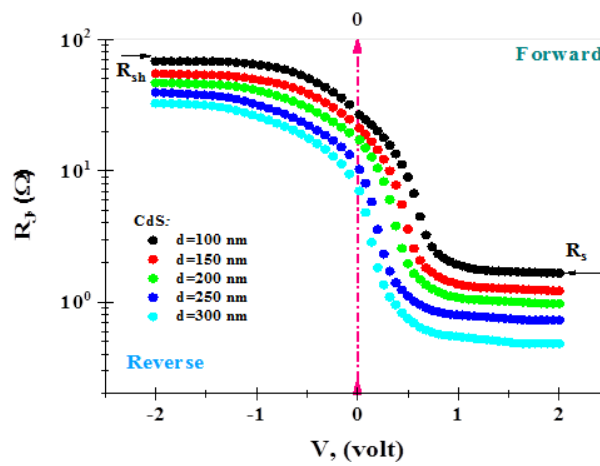


Fig. 9. Heterojunction resistance for the fabricated solar cells.

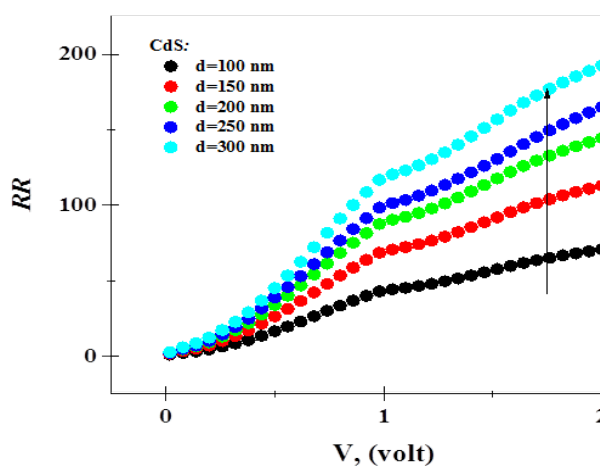


Fig. 10. Rectification rate for the fabricated solar cells.

3.6. Illuminated (I-V) and (P-V) characteristics

Fig. 11 (a, b) portrays the illuminated $I-V$ characteristics of CdS/AgSe/CdTe solar cells with CdS-layer at different thicknesses. On other side, Fig. 12 (a, b) incarnates the illuminated $P-V$

characteristics. The open-circuit voltage V_{OC} and the short-circuit current I_{SC} are determined from Fig. 12 (b). Thus, the power conversion efficiency (PCE) is computed from the following formula [54, 22]:

$$PCE = \left(\frac{P_{max}}{P_{in}} \right) \% \tag{8}$$

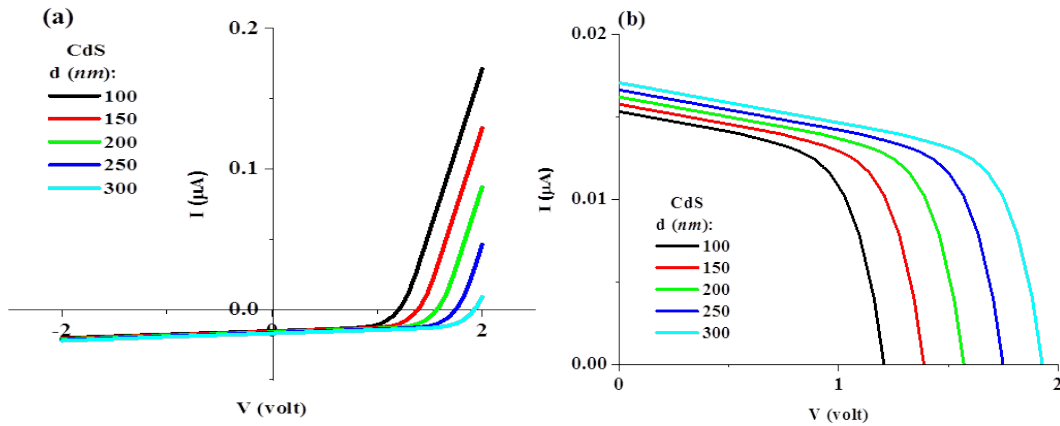


Fig. 11. Illuminated (I - V) curves for the fabricated solar cells.

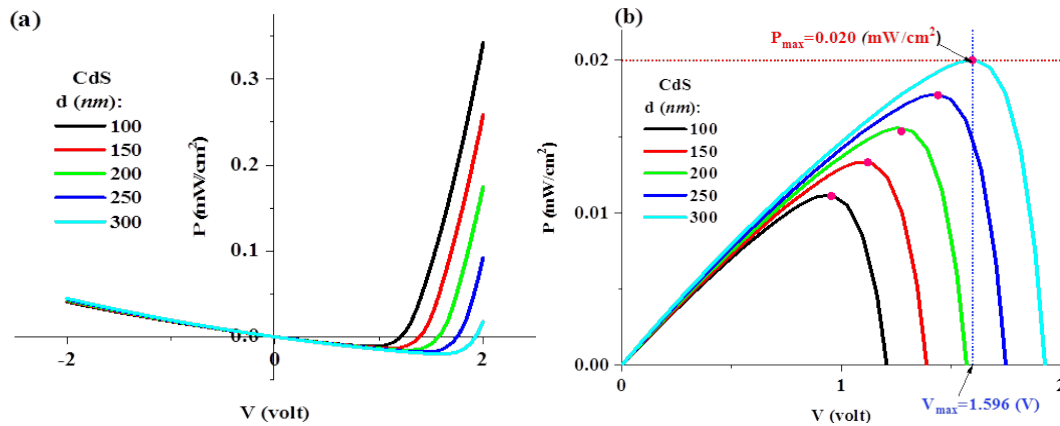


Fig. 12. Illuminated P - V curves for the fabricated solar cells.

As well, solar cells rely on a critical factor known as the "fill factor," which is described as the ratio of maximum attainable power to the ratio of open circuit voltage and short circuit current, as shown below [54, 22]:

$$FF = \left(\frac{V_{max} I_{max}}{V_{oc} I_{sc}} \right) = \frac{P_{max}}{V_{oc} I_{sc}} \tag{9}$$

The obtained values for all mentioned parameters are summarized in Table 2. One can see that the highest (PCE) is 38.48% for CdS-layer with 300 nm according to the listed values in the mentioned table. We think that the high value of transmission and lower reflection spectra at this thickness of CdS-layer are responsible for the improved device performance. Besides, the I_{sc} of solar devices at 300 nm is slightly higher than that of the rest layers. This behavior may be due to the improvement of optoelectronic properties because the larger amounts of photons are absorbed

into CdS/AgSe/CdTe solar cells due to the decrease of reflectance, which leads to the generation of more photo generated carriers in absorber layer and further enhances V_{oc} and I_{sc} . In addition, the possible reason for the relatively high V_{oc} and I_{sc} may be due to the better crystal quality and larger grain size, as well as lower resistivity. The lower resistivity of 300 nm CdS-layer compared with the rest layer also contributes to the improvement of the FF . This is due to decrease resistance of CdS/AgSe/CdTe solar cells. Combining with the above analysis, it can be concluded that 300 nm CdS-layer is beneficial for the improvement of PEC for CdS/AgSe/CdTe solar cells.

Table 2. Dark and illumination parameters of the fabricated solar cells.

d (nm)	Experimental parameters								
	$R_s(\Omega)$	$R_{sh}(\Omega)$	V_{oc} (V)	I_{sc} (mA)	V_{max} (V)	I_{max} (mA)	P_{max} (mW/cm ²)	FF	$PCE\%$
100	1.74	74.68	1.262	0.0153	0.954	0.0116	0.0111	57.447	21.345
150	1.29	58.48	1.425	0.0157	1.120	0.0118	0.0133	59.301	25.595
200	1.04	49.14	1.579	0.0162	1.273	0.0121	0.0153	60.002	29.498
250	0.77	42.84	1.763	0.0166	1.439	0.0123	0.0177	60.429	34.071
300	0.52	34.44	1.935	0.0171	1.596	0.0125	0.0201	60.655	38.483

3.7. Photoresponsivity \mathfrak{R} and quantum efficiency η

In a wide spectral range (100-1000 nm), the photoresponsivity \mathfrak{R} and quantum efficiency η of the device fabricated at different thicknesses of CdS-layer are determined. The ultimate purpose of such determination is to find out which spectral region exhibits strong and desirable spectral properties of the fabricated device (the photo-response characteristics). These quantities are extracted by the following two highlighted equations [55] (see Fig. 13 (a, b)):

$$\mathfrak{R} = \left(\frac{I_{Ph}}{P_{out}} \right) \quad (10)$$

$$\eta\% = \left(\frac{(1.24 \times 10^{-5}) \times \mathfrak{R}}{\lambda} \right) \quad (11)$$

where, I_{Ph} incarnates the photocurrent flowing between the contact electrodes, P_{out} represents the output power and λ portrays the incident light wavelength. The greatest photoresponsivity for a CdS-layer at (300 nm) is 0.367 (A/W), which corresponds to $\lambda_{max} = 654.2$ nm. Thus, as the thickness of the CdS-layer is increased from 100 to 300 nm, the photoresponsivity improves from 0.351 to 0.367 (A/W). This is related to a drop in light absorption intensity and an increase in layer recombination. Furthermore, when the CdS-layer thickness increases, the response intensity increases due to an expansion in free carrier concentration and the potential barrier of the heterojunction device [56, 57].

Furthermore, as illustrated in Fig. 13 (b), the quantum efficiency, η of the manufactured system is evaluated as a function of incident light wavelength in the range of (100-1000 nm). One can be noticed that the value of quantum efficiency shifts toward the higher wavelength as the thickness of the CdS-layer increases. This behavior improves the optical, structural, electrical, and optoelectronic properties for the fabricated solar cells.

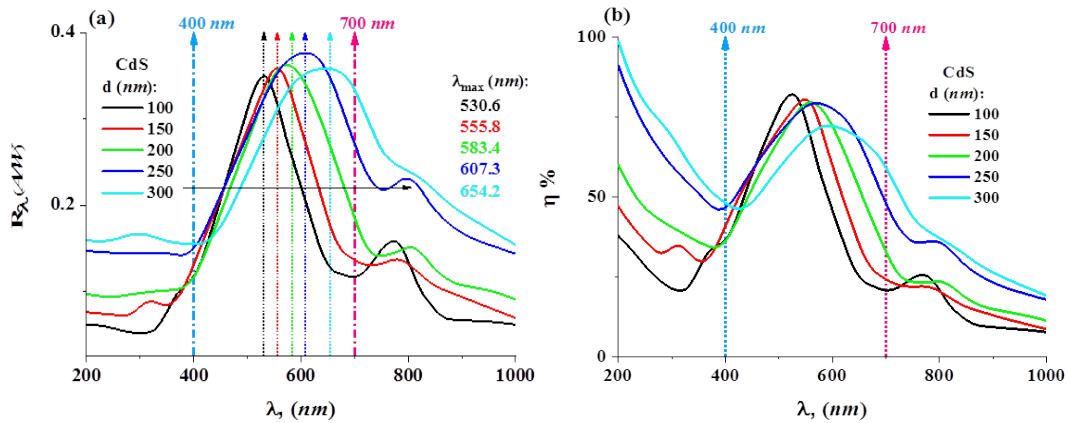


Fig. 13. The photoresponsivity \mathcal{R} and quantum efficiency η of the fabricated devices.

3.8. Dependence of generated photocurrent on light intensity

To determine the relationship of the photocurrent to the bias voltage (for CdS-layer at 300 nm) and the resulting behavior of the electric field strength that can move the charge carriers and thus characterize the depletion region in terms of whether it is wide or not, we represented the relationship of the reversed photocurrent with light intensity as demonstrated in Fig. 14 (a). From this figure, one can discern that the reverse photocurrent increases with increasing both the light intensity and the reverse bias voltage. This means that the fabricated device at a low bias voltage generates a low and not strong electric field and therefore cannot move the charges sufficiently and consequently a narrowing of the depletion region and therefore the magnitude of charge generation and recombination is very small. On the other hand, we can observe that the increase in the photocurrent with an increase in the bias voltage leads steadily to an increase in the exposure of the depletion region, and this is followed by a noticeable increase in the generation of electron-hole pair, and thus improving the photovoltaic properties. The results of this work are consistent with the results of other works included in the corresponding references [58-60].

3.9. Dependence of the generated photocurrent on wavelength (λ)

The dependency of the produced photocurrent on the incident wavelength at ($V_R=2$ volt and $d=300$ nm for CdS-layer) for the manufactured structure before and after illumination is shown in Fig. 14 (b). As compared to the response in the case of light, the response of the studied system seems to be a constant amount in general in dark conditions. This diagram shows that the highest photocurrent occurs at (509.31 nm) due to an improvement in the transmittance spectrum of the CdS layer at this maximum wavelength, which causes more electron-hole pairs to be generated in the depletion layer. This finding is in agreement with the results in the corresponding references [58, 61].

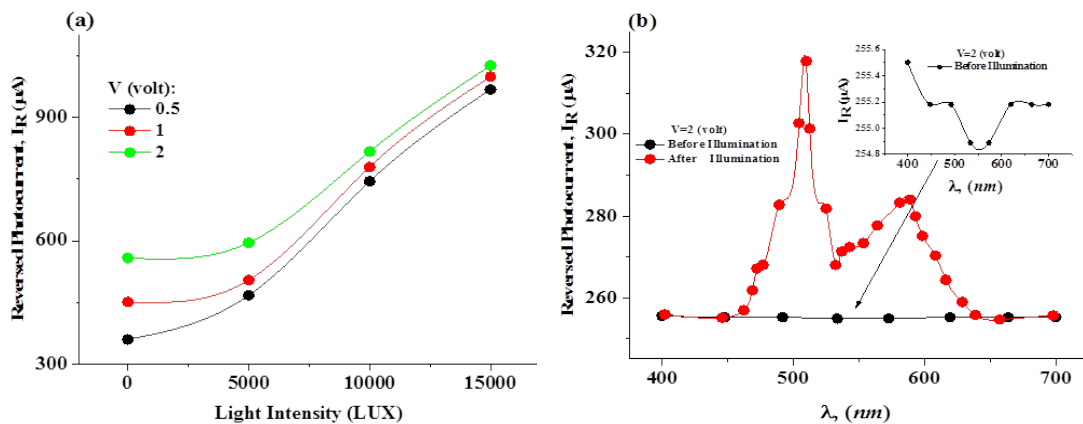


Fig. 14. a) I_R versus light intensity b) I_R versus wavelength for the fabricated solar cell at 300 nm.

4. Conclusions

The crystallization size increased in the current investigation, which was validated using the X-ray method. The photovoltaic aspects were also well-represented in this work. The dark (current-voltage) characteristics of the fabricated device being investigated, as well as the parameters of solar devices under forward and reverse bias for the illumination conditions were extracted. Namely, the current-voltage and power-voltage properties of illumination conditions were investigated. In this case, the open-circuit voltage, the short-circuit current, the fill factor, the power conversion efficiency, (*PCE*), photoresponsivity, quantum efficiency, dependence of generated photocurrent on the light intensity, dependence of the generated photocurrent on wavelength (λ) for the studied solar cell are computed and discussed. The highest energy conversion efficiency was obtained for the thin layer with a thickness of 300 nm, and the value was about 38.48%, which is a high value if compared to previous studies.

Acknowledgments

The researchers wish to extend their sincere gratitude to the Deanship of Scientific Research at the Islamic University of Madinah for the support provided to the post-Publishing.

References

- [1] Hirshman, W. P., Photon International (2010): 176-199.
- [2] Sharma, A., IMS Research (2011): 90-95.
- [3] X. Mathew, J. Pantoja Enriquez, A. Romeo, A.N. Tiwari, Sol. Energy 77, 831 (2004); <https://doi.org/10.1016/j.solener.2004.06.020>
- [4] R. K. Sharma, K. Jain, A.C. Rastogi, Curr. Appl. Phys. 3, 199 (2003); [https://doi.org/10.1016/S1567-1739\(02\)00201-8](https://doi.org/10.1016/S1567-1739(02)00201-8)
- [5] B. Ullrich, J. W. Tomm, N. M. Dushkina, Y. Tomm, H. Sakai, Y Segawa, Solid State Commun. 116, 33 (2000); [https://doi.org/10.1016/S0038-1098\(00\)00267-2](https://doi.org/10.1016/S0038-1098(00)00267-2)
- [6] Han, J., Spanheimer, C., Haindl, G., Fu, G., Krishnakumar, V., Schaffner, J., Fan, C., Zhao, K., Klein, A., Jaegermann, W.: Sol. Energy Mater. Sol. Cells, 95, 816 (2011); <https://doi.org/10.1016/j.solmat.2010.10.027>
- [7] Kim, H., Kim, D.: Sol. Energy Mater. Sol. Cells, 67(1-4), 297 (2001); [https://doi.org/10.1016/S0927-0248\(00\)00295-6](https://doi.org/10.1016/S0927-0248(00)00295-6)
- [8] Amin, N., Sopian, K., Konagai, M., Sol. Energy Mater. Sol. Cells, 91, 1202 (2007); <https://doi.org/10.1016/j.solmat.2007.04.006>
- [9] ER Shaaban, MS Abd El-Sadek, M El-Hagary, IS Yahia, Physica Scripta 86 (1) (2012) 015702; <https://doi.org/10.1088/0031-8949/86/01/015702>
- [10] Chari F. T. and Fadavieslam M. R., Optical and Quantum Electronics, 51(377), 1-16(2019).
- [11] Buckingham M. A., Catherall A. L., Hill M. S., Johnson A. L., and Parish J. D., Crystal Growth & Design, 17(2), 907-912(2017); <https://doi.org/10.1021/acs.cgd.6b01795>
- [12] Rodríguez-Mas F., Ferrer J. C., Alonso J. L. and Fernández de Ávila S., Nanomaterials, 9(1212), 1-19 (2019); <https://doi.org/10.3390/nano9091212>
- [13] K. Senthil, D. Mangalraj, S. K. Narayandass, Appl. Surf. Sci.169, 476 (2001); [https://doi.org/10.1016/S0169-4332\(00\)00732-7](https://doi.org/10.1016/S0169-4332(00)00732-7)
- [14] P. Taneja, P. Vasa, P. Ayyub, Mater. Lett. 54, 343 (2002); [https://doi.org/10.1016/S0167-577X\(01\)00590-0](https://doi.org/10.1016/S0167-577X(01)00590-0)
- [15] EIS Yousef, A. El-Adawy, N. El Koshkhany, E. R. Shaaban, Journal of Physics and Chemistry

- of Solids., 67(2006)1649-1655; <https://doi.org/10.1016/j.jpics.2006.02.014>
- [16] M.C. Baykul, A. Balcioglu, *Microelectron. Eng.* 51, 703 (2000); [https://doi.org/10.1016/S0167-9317\(99\)00534-1](https://doi.org/10.1016/S0167-9317(99)00534-1)
- [17] M. Tsuji, T. Aramoto, H. Ohyama, T. Hibino, K. Omura, *J. Cryst. Growth* 214, 1142 (2000); [https://doi.org/10.1016/S0022-0248\(00\)00291-8](https://doi.org/10.1016/S0022-0248(00)00291-8)
- [18] J. Nishino, S. Chatani, Y. Uotani, Y. Nosaka, *J. Electroanal. Chem.* 473, 217 (1999); [https://doi.org/10.1016/S0022-0728\(99\)00250-8](https://doi.org/10.1016/S0022-0728(99)00250-8)
- [19] R. Padmavathy, N.P. Rajesh, A. Arulchakkaravarthi, R. Gopalakrishnan, P. Santharaghavan, P. Ramasamy, *Mater. Lett.* 53, 321 (2002); [https://doi.org/10.1016/S0167-577X\(01\)00500-6](https://doi.org/10.1016/S0167-577X(01)00500-6)
- [20] Bonnet, D., and H. Rabenhorst., *Photovoltaic Specialists Conference*, 9 th, Silver Spring, Md. 1972.
- [21] He, S., Lu, H., Li, B., Zhang, J., Zeng, G., Wu, L., Feng, L., *Materials Science in Semiconductor Processing* 67 (2017): 41-45; <https://doi.org/10.1016/j.mssp.2017.05.009>
- [22] Qasem, A., Alrafai, H. A., Alshahrani, B., Said, N. M., Hassan, A. A., Yakout, H. A., & Shaaban, E. R., *Journal of Alloys and Compounds* (2021): 163374; <https://doi.org/10.1016/j.jallcom.2021.163374>
- [23] Shaaban, E. R., Osman, M. A., Osman, A. A., Sayed, M. M., & Aly, K. I, *Journal of Materials Science: Materials in Electronics* (2022): 1-13.
- [24] H. M Rietveld, *J. Appl. Crystallogr.* 2 (1969) 65-71; <https://doi.org/10.1107/S0021889869006558>
- [25] R. Devi, P. K. Kalita, P. Purakayastha, and B. K. Sarma., *J. Optoelectron. Adv. Mater.*, 10(11) (2008) 3077.
- [26] Qasem, A., Mostafa, M. S., Yakout, H. A., Mahmoud, M., & Shaaban, E. R., *Optics & Laser Technology* 148 (2022): 107770; <https://doi.org/10.1016/j.optlastec.2021.107770>
- [27] Qasem, A., Said, N. M., Hassan, A. A., Yakout, H. A., & Shaaban, E. R., *Physica B: Condensed Matter* (2021): 413600; <https://doi.org/10.1016/j.physb.2021.413600>
- [28] Qasem, A., Hassan, A. A., Rajhi, F. Y., Abbas, H. A. S., & Shaaban, E. R., *Journal of Materials Science: Materials in Electronics* (2021): 1-13.
- [29] ER Shaaban, Mansour Mohamed, Mohamed N Abd-el Salam, AY Abdel-Latif, MA Abdel-Rahim, *Optical Materials*, 86 (2018) 318-325; <https://doi.org/10.1016/j.optmat.2018.10.027>
- [30] Ashutosh Goel, Dilshat U Tulyaganov, Anna Maria Ferrari, Essam R Shaaban, Andreas Prange, Federica Bondioli, José MF Ferreira, *Journal of the American Ceramic Society*, 93(3) (2010) 830-837. <https://doi.org/10.1111/j.1551-2916.2009.03503.x>
- [31] K. Senthil, D. Mangalaraj, K. Narayandass, *Appl. Surf. Sci.*, 169-170 (2001) 476; [https://doi.org/10.1016/S0169-4332\(00\)00732-7](https://doi.org/10.1016/S0169-4332(00)00732-7)
- [32] ER Shaaban, IS Yahia, M Fadel, *Journal of alloys and compounds* 469 (1-2) (2009) 427-432; <https://doi.org/10.1016/j.jallcom.2008.01.155>
- [33] H. Fujiwara, *Spectroscopic Ellipsometry Principles and Applications*, John Wiley & Sons Ltd, West Sussex, England, 2007; <https://doi.org/10.1002/9780470060193>
- [34] M. Emam-Ismael, M. El-Hagary, H. M. El-Sherif, A. M. El-Nagga, M. M. El-Nahass, *Opt. Mater.* 112 (2021) 110763; <https://doi.org/10.1016/j.optmat.2020.110763>
- [35] A. Segura, J. P. Guesdon, J. M. Besson, & A. Chevy, *Journal of applied physics* 54.2 (1983): 876-888; <https://doi.org/10.1063/1.332050>
- [36] Yazawa, Kazuaki, Je-Hyeong Bahk, and Ali Shakouri. *Thermoelectric Energy Conversion Devices and Systems*. Vol. 7. World Scientific, 2021; <https://doi.org/10.1142/11770>
- [37] Mansour Mohamed, ER Shaaban, Mohamed N Abd-el Salam, AY Abdel-Latif, Safwat A Mahmoud, MA Abdel-Rahim, *Optik* 178 (2019)1302-1312; <https://doi.org/10.1016/j.ijleo.2018.10.103>
- [38] Levin, E. M. "Charge carrier effective mass and concentration derived from combination of Seebeck coefficient and Te 125 NMR measurements in complex tellurides." *Physical Review B*

- 93.24 (2016): 245202; <https://doi.org/10.1103/PhysRevB.93.245202>
- [39] ER Shaaban, *Physica B: condensed matter* 373 (2), 211-216; <https://doi.org/10.1016/j.physb.2005.11.145>
- [40] Askari, M., Soltani, N., Saion, E., Yunus, W. M. M., Erfani, H. M., & Dorostkar, M, *Superlattices Microstruct.* 81 (2015) 193-201; <https://doi.org/10.1016/j.spmi.2015.01.011>
- [41] Xie, R., Su, J., Liu, Y., & Guo, L, *Int. J. Hydrog. Energy* 39 (7) (2014) 3517-3527; <https://doi.org/10.1016/j.ijhydene.2013.12.088>
- [42] Haeffler, G., Klinkmüller, A. E., Rangell, J., Berzinsh, U., & Hanstorp, D. *Molecules and Clusters* 38.3 (1996): 211-214; <https://doi.org/10.1007/s004600050085>
- [43] Ferro, R., and J. A. Rodriguez. *Solar energy materials and solar cells* 64.4 (2000): 363-370; [https://doi.org/10.1016/S0927-0248\(00\)00228-2](https://doi.org/10.1016/S0927-0248(00)00228-2)
- [44] A Arora, A Goel, ER Shaaban, K Singh, OP Pandey, JMF Ferreira, *Physica B: Condensed Matter* 403 (10-11), 1738-1746; <https://doi.org/10.1016/j.physb.2007.10.001>
- [45] Chaibi, W., Peláez, R. J., Blondel, C., Drag, C., & Delsart, C. *The European Physical Journal D* 58.1 (2010): 29-37; <https://doi.org/10.1140/epjd/e2010-00086-7>
- [46] Lang, Peter F., and Barry C. Smith. *Journal of chemical education* 80.8 (2003): 938; <https://doi.org/10.1021/ed080p938>
- [47] A Goel, DU Tulyaganov, MJ Pascual, ER Shaaban, F Muñoz, Z Lü, José MF Ferreira *Journal of non-crystalline solids* 356 (20-22) (2010) 1070-1080; <https://doi.org/10.1016/j.jnoncrysol.2010.01.012>
- [48] Maurya, Ram Charitra. "Appendix I. Inorganic Chemistry. De Gruyter, 2021. 563-576.
- [49] Vandevraye, Mickaël, Cyril Drag, and Christophe Blondel. *Physical Review A* 85.1 (2012): 015401; <https://doi.org/10.1103/PhysRevA.85.015401>
- [50] Bratsch, Steven G., and J. J. Lagowski, *Polyhedron* 5 (11) (1986) 1763-1770; [https://doi.org/10.1016/S0277-5387\(00\)84854-8](https://doi.org/10.1016/S0277-5387(00)84854-8)
- [51] Alshahrani, B., Nabil, S., Elsaedy, H. I., Yakout, H. A., & Qasem, A., *Journal of Electronic Materials* (2021): 1-13.
- [52] Qasem, A., Mahmoud, M., Elsaedy, H. I., Mostafa, M. S., & Shaaban, E. R., *Optical Materials* (2021): 111746; <https://doi.org/10.1016/j.optmat.2021.111746>
- [53] D Prakash, AM Aboraia, M El-Hagary, ER Shaaban, KD Verma, *Ceramics International* 42 (2) (2016) 2676-2685; <https://doi.org/10.1016/j.ceramint.2015.10.096>
- [54] Elsaedy, H. I., Qasem, A., Yakout, H. A., & Mahmoud, M., *Journal of Alloys and Compounds* 867 (2021): 159150; <https://doi.org/10.1016/j.jallcom.2021.159150>
- [55] Qasem, A., Alshahrani, B., Yakout, H. A., Abbas, H. A. S., & Shaaban, E. R., *Applied Physics A* 127.11 (2021): 1-13; <https://doi.org/10.1007/s00339-021-04999-4>
- [56] S. Manna, S. Das, S. P. Mondal, R. Singha & S. K. Ray, *J. Phys. Chem. C* 116 (2012) 7126-7133; <https://doi.org/10.1021/jp210455w>
- [57] Hussein, Hasan I., Auday H. Shaban, and Iman H. Khudayer, *Energy Procedia* 157 (2019) 150-157; <https://doi.org/10.1016/j.egypro.2018.11.175>
- [58] AH AL-abbasy, Bashar, *Al-Rafidain Engineering Journal (AREJ)* 19.2 (2011): 68-76; <https://doi.org/10.33899/rengj.2011.27347>
- [59] Ponpon, 9_JP., *Solid-state electronics* 28.7 (1985): 689-706; [https://doi.org/10.1016/0038-1101\(85\)90019-X](https://doi.org/10.1016/0038-1101(85)90019-X)
- [60] Joshi, N. V., and Alicia Serfaty., *International journal of infrared and millimeter waves* 10.9 (1989): 1077-1088; <https://doi.org/10.1007/BF01010366>
- [61] Poortmans, Jef, and Vladimir Arkhipov, eds. *Thin film solar cells: fabrication, characterization and applications*. Vol. 18. John Wiley & Sons, 2006; <https://doi.org/10.1002/0470091282>